Spherical Wave Channel and Analysis for Large Linear Array in LoS Conditions

Zhou, Zhou; Gao, Xiang; Fang, Jun; Chen, Zhi

Published in:
2015 IEEE Globecom Workshops (GC Wkshps)

DOI:
10.1109/GLOCOMW.2015.7414041

2015

Spherical Wave Channel and Analysis for Large Linear Array in LoS Conditions

Zhou Zhou*, Xiang Gao†, Jun Fang* and Zhi Chen*
*National Key Laboratory on Communications, University of Electronic Science and Technology of China, Chengdu, China
†Department of Electrical and Information Technology, Lund University, Sweden
Email: zhouzhou@std.uestc.edu.cn, xiang.gao@eit.lth.se, junfang@uestc.edu.cn, chenzhi@uestc.edu.cn

***Abstract*—Massive MIMO is considered a key technology for the future wireless communication systems. The promising properties in terms of higher spectral and transmit-energy efficiency are brought by the large number of antennas at the base station (BS). As the number of antennas increases, the aperture of the BS antenna array may become much larger, as compared to today's antenna arrays. In this case, mobile stations (MSs) and significant scatterers can locate inside the Rayleigh distance of large arrays, and spherical wavefronts rather than planar wavefronts are experienced over the arrays. In this paper, we propose an analytical spherical-wave channel model for large linear arrays, which is also compatible with conventional plane-wave models. Based on the spherical-wave model, we investigate how MSs can be spatially separated in simple line-of-sight (LoS) scenarios. The results theoretically explain the observation in experiments that spherical wavefronts help decorrelate the MS channels more effectively than planar wavefronts.**

I. Introduction

With the advent of massive MIMO [1], [2] for providing a large spatial degrees of freedom, it comes to the questions of better analyzing and modeling the spatial properties of the radio channels. Classical MIMO channel models are usually based on the planar wavefront assumption, and can provide performance prediction in both line-of-sight (LoS) and non-line-of-sight (NLoS) channel conditions [3]. However, as shown in recent massive MIMO studies based on channel measurements, the plane-wave assumption does not hold for physically-large arrays [4]–[8]. When the number of antennas at the base station (BS) increases to hundreds, the aperture of the antenna array may become much larger, as compared to conventional MIMO. In this case, mobile stations (MS) and scatterers most likely locate inside the Rayleigh distance of the large arrays.

The radiation field of antennas is usually divided into two regions, the near-field region (Fresnel zone) and the far-field region (Fraunhofer zone) [9]. The boundary between the two regions is approximately the Rayleigh distance [10],

$$Z = \frac{2D^2}{\lambda}, \tag{1}$$

where D is the maximum dimension of the antenna or antenna array, and λ represents the wavelength. In conventional MIMO systems, for example, with up to 8 antennas in LTE [11], we usually assume that the locations of MSs and scattering objects are far beyond the Rayleigh distance of the BS antenna array, i.e., $d \gg Z$, where d is the distance between the MSs or scatterers and the BS. In far-field region, the plane-wave assumption is well-reasoned for MIMO channel models [12]. However, in massive MIMO with physically-large arrays, the Rayleigh distance Z becomes large as the array aperture D increases, thus we may have $d < Z$ or $d \approx Z$. For example, in a semi-urban channel measurement campaign in the 2.6 GHz band, as reported in [6] and [7], a 7.4 m uniform linear array was deployed at the BS, giving the Rayleigh distance about 950 m. All the MSs and significant scatterers are within this distance. Spherical wavefronts over the large array were observed, by referring to the angular power spectrum over the array in the measured channels [4]. Therefore, planar wavefront assumptions for conventional MIMO channels are not suitable for physically-large arrays in massive MIMO scenarios.

Motivated by the experimental results on massive MIMO channels, the characteristics of the near-field propagation, i.e., spherical wavefronts over large arrays, should be taken into consideration when analyzing and modeling massive MIMO channels. In [13], the early research on MIMO capacity considers spherical-wave aware models and briefly exploits the relationship between channel capacity and array geometries. In [14], the study empirically shows that spherical-wave model is more accurate than plane-wave model for short-range MIMO performance estimation, if the distance between the transmitter and receiver is below the Rayleigh distance. Besides short-range communication, [15] and [16] also consider spherical wavefronts, and propose a technique for realizing high-rank channel matrix in pure LoS conditions and thus achieving high channel capacity, by optimizing antenna placement in uniform linear arrays.

In this work, we propose an analytical channel model for physically-large linear arrays, which takes spherical wavefronts into consideration. We characterize the spherical-wave channel steering vector by a group of geometrical parameters. The spherical-wave model is formulated in a general form, and the closed-form steering vector can be easily used for analytical study and extended to other types of antenna arrays. Based on this, we show that our model is compatible with the conventional plane-wave model. We theoretically study how the number of BS antennas, antenna spacing and MS spacing affect the spatial separability of the MSs in LoS conditions. We also demonstrate how spherical wavefronts help decorrelate the MS channels, especially for closely-spaced MSs. This effect has been observed but is not explicit in previous studies based on measured channels [4], [7].

The rest of the paper is organized as follows. In Sec. II, we propose and formulate our spherical-wave channel model. Then Sec. III and IV present theoretical analysis and simulation results, respectively. Finally, Sec. V summarizes the paper.

II. Spherical-wave Channel Model

We first consider the channel from single-antenna MSs to multiple-antenna BS with LoS components only, then we make an extension by adding a reflected path to the pure LoS channel.

A. Basic Model

Fig. 1 depicts the established coordinate system of the spherical-wave channel model. We arbitrarily choose one antenna position on the array at the BS side as the origin. The number of antennas is N_r+1, and the antenna index i ranges from $-\delta N_r$ to $(1-\delta)N_r$, where $\delta>0$ is defined as the *antenna index parameter* and depends on the location of the origin. In the figure, $\theta\in[0,\pi]$ is the angle of incidence from the MS to the antenna at the origin, Δ_r is the normalized BS antenna spacing in wavelength λ_c, d is the distance from the MS to the origin, and φ_i (namely angle variation) is the included angle between the MS-origin direction and the direction of the MS to the ith-antenna.

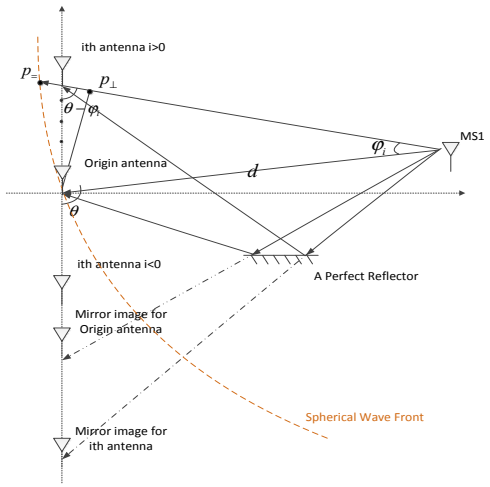

Fig. 1. Illustration of the spherical-wave model. The effect of a perfect reflector is equivalent to having "virtual" BS antennas that are mirrored by the reflector.

We first consider free-space transmission with only LoS components in the radio channel. This means that there is no scattering in the channel thus no small-scale or large-scale fading. Hence, the spherical-wave eigenmode for the channel coefficient h between the MS and the origin antenna is

$$h\propto\frac{1}{d}e^{-j\frac{2\pi}{\lambda}d}, \tag{2}$$

where $1/d$ is the factor due to the free-space pathloss. After some calculations in geometry, the corresponding spherical-wave channel vector can be expressed as

$$\mathbf{h}^H\propto\left[\ \frac{e^{j\frac{2\pi}{\lambda_c}L_{-\delta N_r}}}{L_{-\delta N_r}}\quad\frac{e^{j\frac{2\pi}{\lambda_c}L_{-\delta N_r+1}}}{L_{-\delta N_r+1}}\quad\cdots\quad\frac{e^{j\frac{2\pi}{\lambda_c}L_{(1-\delta)N_r}}}{L_{(1-\delta)N_r}}\ \right], \tag{3}$$

where

$$L_i=\begin{cases}\Delta_r\lambda_c i\cos(\theta-\varphi_i)+\cos(\varphi_i)d, & i\geq 0\\ \Delta_r\lambda_c i\cos(\theta+\varphi_i)+\cos(\varphi_i)d, & i<0\end{cases} \tag{4}$$

and

$$\varphi_i(\Delta_r,d,\theta)=\begin{cases}\arctan(\frac{r_i}{1+c_i}), & i\geq 0\\ \arctan(-\frac{r_i}{1+c_i}), & i<0\end{cases}, \tag{5}$$

$r_i=\frac{\Delta_r i\lambda_c\sin(\theta)}{d}$, $c_i=\frac{\Delta_r i\lambda_c\cos(\theta)}{d}$, and $\arctan(\cdot)$ is the arctangent function defined in interval $[0,\pi]$. Note that L_i and φ_i indicate the phase variation and angle variation over the array, respectively.

Let us define the steering vector as the normalized channel vector

$$\mathbf{a}(\boldsymbol{\varpi})=\frac{\mathbf{h}}{\|\mathbf{h}\|}, \tag{6}$$

where $\boldsymbol{\varpi}\triangleq(d,\theta,\delta;N_r,\Delta_r)$. Note that δ and θ are not fully independent. It is interesting to compare this spherical-wave steering vector with the conventional MIMO steering vector that assumes planar wavefronts [12], i.e.,

$$h_i\propto\frac{1}{d}e^{-j2\pi\Delta_r i\cos(\theta)}, \tag{7}$$

where $i\in[0,N_r]$. Different from the plane-wave model, the phase variation and pathloss variation over the array are nonlinear in the spherical-wave model, as shown in (3). The spherical-wave model is more general, and we will show in Sec. III that it can be approximated to the plane-wave model when BS-MS distance is large ($d\gg Z$).

B. Choice of Origin

With the defined spherical-wave steering vector in (6), one issue is how to choose the ordinate origin. In general, for each MS, we can choose a different antenna position on the array as the origin, and derive the relation between the parameters for different MSs. For example, for two groups of parameters $\boldsymbol{\varpi}_1=(d_1,\theta_1,\delta_1;N_r,\Delta_r)$ and $\boldsymbol{\varpi}_2=(d_2,\theta_2,\delta_2;N_r,\Delta_r)$ of the same channel vector, i.e., $\mathbf{h}(\boldsymbol{\varpi}_1)=\mathbf{h}(\boldsymbol{\varpi}_2)$, assuming $\delta_1>\delta_2$, the angle variation $\varphi_{1,i}$ and $\varphi_{2,i}$, where $i\in[-\delta_k N_r,(1-\delta_k)N_r]$, $k=1,2$, follow the relation

$$\varphi_{1,i}=\varphi_{2,i+(\delta_1-\delta_2)N_r}, \tag{8}$$

for $\forall i\in[-\delta_1 N_r,(1-\delta_1)N_r]$.

In this paper, we have two choices of the coordinate origin for different purposes of analysis. The two choices are as follows.

1) The first antenna position is set as the origin, thus we have $\delta=0$ and $\boldsymbol{\varpi}=(d,\theta,0;N_r,\Delta_r)$. With this setting, we demonstrate that the proposed model is compatible with the conventional plane-wave model in Sec. III.
2) We set the origin at the antenna position that is close to the point of the normal incidence from the MS to the BS antenna array, so $\boldsymbol{\varpi}=(d,\frac{\pi}{2},\delta';N_r,\Delta_r)$, where δ' is the corresponding antenna index paramter. Without loss of generality, we assume there is always an antenna

position at the point of the normal incidence. Therefore, using (4) and (5), we have

$$L_i = \sqrt{(\Delta_r \lambda_c i)^2 + d^2}\,\sin(\varphi_i + \omega_i), \tag{9}$$

$\varphi_i = \arctan(\left|\frac{\Delta_r \lambda_c i}{d}\right|)$, $\omega_i = \arccos(\frac{|\Delta_r \lambda_c i|}{\sqrt{(\Delta_r \lambda_c i)^2 + d^2}})$, for $i \in [-N_r\delta', N_r(1-\delta')]$. Since $\varphi_i + \omega_i = \frac{\pi}{2}$, (9) is simplified to

$$L_i = \sqrt{(\Delta_r \lambda_c i)^2 + d^2}. \tag{10}$$

By using (10), the analysis of the orthogonality between different MS channels is tractable, and we present the analysis results in Sec. III.

C. Model Extension

The proposed model can be easily extended from single-user to multi-user case. With N_t single-antenna users, the channel matrix is

$$\mathbf{H} \propto \left[\begin{array}{cccc} \mathbf{h}(\boldsymbol{\varpi}_1) & \mathbf{h}(\boldsymbol{\varpi}_2) & \ldots & \mathbf{h}(\boldsymbol{\varpi}_{N_t}) \end{array}\right], \tag{11}$$

where $\mathbf{h}(\boldsymbol{\varpi_k})$ is the channel vector of the kth MS to the BS.

We can also extend the model to include a perfect reflector, as illustrated in Fig. 1. The effect of the reflection path is equivalent to having "virtual" BS antennas that are mirrored by the perfect reflector (see Fig. 1). We can see this effect as increasing the number of BS antennas. Using the principle of superposition [12], the channel vector becomes

$$\mathbf{h} \propto \sqrt{\kappa}\mathbf{h}(N_r, \Delta_r, d_{r1}, \theta_{r1}) + \mathbf{h}(N_r, \Delta_r, d_{r2}, \theta_{r2}), \tag{12}$$

where the subscript 1 and 2 indicate the actual BS antennas and the virtual BS antennas, respectively, and the first term is the channel of the LoS path, the second term is the channel of the reflected path. The factor κ is the power ratio between the LoS path and the reflected path. Note that d_{r2} and θ_{r2} are calculated according to the principle of specular reflection.

III. Model Analysis

We consider multi-user MIMO (MU-MIMO) with two single-antenna MSs ($N_t = 2$), as illustrated in Fig. 2. The analysis and obtained results can be easily extended to the case of more MSs. In the uplink the received signal at BS can be expressed as

$$\mathbf{y} = \mathbf{h}_1 x_1 + \mathbf{h}_2 x_2 + \mathbf{n}, \tag{13}$$

where x_1, x_2 are the complex transmitted symbols by the two MSs, with the same energy $\mathbb{E}\left\{|x_k|^2\right\} = E_x$. The instantaneous uplink channel capacity is

$$C_{\text{inst}} = \sum_{k=1}^{N_t} \log_2(1 + \frac{E_x}{N_0}\sigma_k^2), \tag{14}$$

where N_0 is the complex Gaussian noise variance, and σ_k is the kth singular value of matrix $\mathbf{H} = [\,\mathbf{h}_1 \;\; \mathbf{h}_2\,]$. It can be proved that C_{inst} reaches the maximum when $\sigma_1 = \sigma_2$. If $\mathbf{h_1}$ and $\mathbf{h_2}$ have the same norm, this condition that $\sigma_1 = \sigma_2$ is called "favorable" propagation conditions that the two MS channels are fully orthogonal [17].

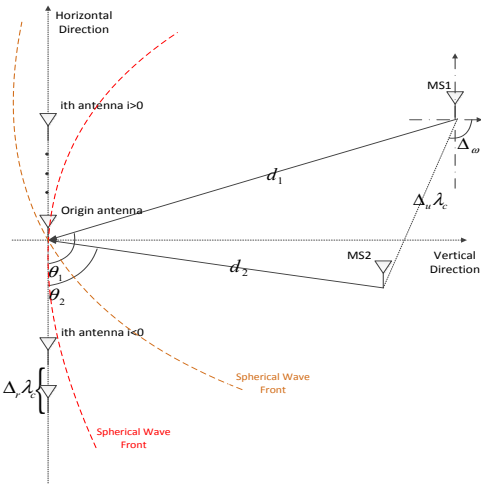

Fig. 2. Illustration of the spherical-wave model with two single-antenna MSs.

Here we assume that the MS channels have the same pathloss, and the channel vectors are normalized, i.e., $\mathbf{h}_k = \mathbf{a}(\boldsymbol{\varpi}_k), k = 1, 2$. Denote the correlation coefficient between the two channels by $f = \left|\mathbf{a}^H(\boldsymbol{\varpi}_1)\mathbf{a}(\boldsymbol{\varpi}_2)\right|$, we have

$$\frac{\sigma_1}{\sigma_2} = \sqrt{\frac{1+f}{1-f}}, \tag{15}$$

where $\sigma_1/\sigma_2 = 1$ if and only if $f = 0$. To reach higher channel capacity, we expect the channel correlation coefficient f to be close to 0. Next, we investigate the correlation between the MS channels in the proposed spherical-wave model.

The channel correlation $f(N_r, \Delta_r, \boldsymbol{\delta}; \theta, d, \Delta_u, \Delta_\omega)$ is a function of a group of geometric parameters. Here we choose different origins for the two MSs, and the geometric parameters for MS 1 is used as a reference to derive the parameters for MS 2, as in this way our theoretical analysis can be simplified. Thus, we have the antenna index parameter $\boldsymbol{\delta} = (\delta_1, \delta_2)$, the BS-MS distance $d = d_1$, the angle of incidence $\theta = \theta_1$, and Δ_u is the spacing between MSs in wavelength, Δ_ω is the included angle between MSs' connecting direction and the vertical direction (see Fig. 2). The geometric parameters for MS 2 are

$$d_2 = \sqrt{d^2 + \Delta_u^2\lambda_c^2 + 2d\Delta_u\lambda_c \sin(\theta - \Delta_\omega)} \tag{16}$$

and

$$\theta_2 = \frac{\pi}{2} - \arctan(\frac{\frac{d}{\Delta_u\lambda_c}\cos(\theta) - \sin(\Delta_\omega)}{\frac{d}{\Delta_u\lambda_c}\sin(\theta) + \cos(\Delta_\omega)}). \tag{17}$$

In the far-field region and when the MS spacing is too small, i.e., $d \gg \Delta_u\lambda_c$, from (17) we have $\theta_1 - \theta_2 \to 0$, where it is difficult to spatially separate the MSs as the angles of arrival are similar. However, in the near-field region, even if the MS spacing is small, it is possible to spatially separate the MSs due to spherical wavefronts are experienced over the array. We show this effect later in this section.

Using the relation in (8), we can decompose the channel correlation coefficient

$$f(N_r, \Delta_r, \boldsymbol{\delta}; \theta, d, \Delta_u, \Delta_\omega) = \left| \sum_{i=-\delta_1 N_r}^{(1-\delta_1)N_r} f_i \right|, \quad (18)$$

where $f_i = a_{1,i}^* a_{2,i}$, $a_{1,i}$ and $a_{2,i}$ are the channel coefficients between the MSs and the ith BS antenna, and satisfies $\angle f_i \propto L_{1,i} - L_{2,i+(\delta_1-\delta_2)N_r}$, $|f_i| \propto 1/|L_{1,i} L_{2,i+(\delta_1-\delta_2)N_r}|$, for $i \in [-\delta_1 N_r, (1-\delta_1)N_r]$. Note that $\angle f_i$ indicates the variation of the phase differences between the two MSs over the array. With relatively large variation in phase difference, we expect relatively better spatial separation of the MS channels.

A. Angle and Phase Variations

In the proposed model, we can see that the angle variation factor φ_i in (5) determines the phase variation over the array, see (3) and (4), and therefore the channel correlation f. We next discuss the angle and phase variations over the array in two extreme cases – when the MSs are very far from the BS and when the MSs are very close to the BS, as follows.

- If the MSs are very far from the BS, i.e., in the far field of the BS antenna array, $d \gg Z$, as discussed in Sec. I, sufficiently we have $d \gg \Delta_r \lambda_c N_r$. In this case, in (5), $r_i \to 0$ and $c_i \to 0$, thus there is neither angle variation nor pathloss difference over the array as

$$\begin{aligned} &\varphi_i(\Delta_r, d, \theta) = 0, \\ &\frac{1}{L_i} \approx \frac{1}{d}. \end{aligned} \quad (19)$$

  The channel steering vector then becomes the conventional steering vector under the assumption of planar wavefronts over the array, as in (7).
- If the MSs are very close to the BS, we have $r_i \to \infty$ and $c_i \to \infty$, resulting in

$$\varphi_i(\Delta_r, d, \theta) = \theta, \quad (20)$$

  and $L_i \propto \Delta_r \lambda_c i$. In this extreme case, there is again no angle variation over the array.

For the phase variation, from (10) we see that when $i \in (0, (1-\delta')N_r]$, L_i monotonically increases with respect to i, and when $i \in [-\delta' N_r, 0)$, monotonically decreases. Thus, L_i is a quasi-convex function of the antenna index i. Generally, for any antenna with incident angle θ, we have $\varphi_{i^*} = \theta - \frac{\pi}{2}$ and $L_{i^*} = d\sin(\theta)$ for some $i^* > 0$ when $\theta > \frac{\pi}{2}$.

B. Phase Difference and Spatial Decorrelation

As explained by (18), the phase difference $\angle f_i$ determines the channel correlation. Here we focus on the geometric factors related to $\angle f_i$ and try to predict the channel correlation. Specifically, we investigate the phase difference $\angle f_i$ in the two extreme cases – when the MSs are very far from or very close to the BS, as follows.

- When $d_1 \ll |\Delta_r \lambda_c i|$ and $d_2 \ll |\Delta_r \lambda_c i|$, using (10) we have

$$\angle f_i \approx \begin{cases} 2\pi\Delta_r(\delta_1' - \delta_2')N_r, & \text{when } i > (\delta_1' - \delta_2')N_r \\ 2\pi\Delta_r(\delta_2' - \delta_1')N_r, & \text{when } i < 0 \\ -4\pi\Delta_r i + 2\pi\Delta_r(\delta_2' - \delta_1')N_r, & \text{others.} \end{cases} \quad (21)$$

The channel correlation f in (18) can also be written as

$$f = \left| \sum_{i=-\delta_1' N_r}^{0} f_i + \sum_{i=1}^{(\delta_1'-\delta_2')N_r} f_i + \sum_{i=(\delta_1'-\delta_2')N_r+1}^{(1-\delta_1')N_r} f_i \right|. \quad (22)$$

We see that if the antenna index i is outside the interval $[1, (\delta_1' - \delta_2')N_r]$, the phase difference $\angle f_i$ remains constant, see (21). These antennas contribute little to reduce the channel correlation f. This indicates that we cannot always separate the MS channels by increasing the number of antennas in this extreme case. Hence, we call this phenomenon as a saturation of phase variation in large number of antennas, when MSs are very close to BS array.

- When $d_1 \gg |\Delta_r \lambda_c i|$ and $d_2 \gg |\Delta_r \lambda_c i|$, we have

$$\angle f_i = 2\pi(\cos\theta_1 - \cos\theta_2)\Delta_r i, \quad (23)$$

  where $i = 0, ..., N_r$, and θ_1 is the angle of incidence from MS 1 to the first antenna, similarly θ_2. We can see that the decorrelation of the MS channels relies on the difference in the angles of incidence. When $\theta_1 = \theta_2$, i.e., two MSs are in the same vertical direction (Fig. 2), $\angle f_i = 0$, it is thus impossible to spatially separate the MSs. In this extreme case that the MSs are very far from the BS, the channel correlation is given by

$$f \propto \left| \frac{\sin(\pi(N_r+1)(\cos\theta_1 - \cos\theta_2)\Delta_r)}{\sin(\pi(\cos\theta_1 - \cos\theta_2)\Delta_r)} \right|, \quad (24)$$

  as discussed in [12].

Generally, in between the two extreme cases, we have spherical wavefronts over the array. From (10), the phase difference $\angle f_i$ over the array can be written as

$$\begin{aligned} \angle f_i \propto &\sqrt{(\Delta_r \lambda_c i)^2 + (d_1)^2} \\ &- \sqrt{(\Delta_r \lambda_c (i + (\delta_1' - \delta_2')N_r))^2 + (d_2)^2}. \end{aligned} \quad (25)$$

We evaluate the phase difference $\angle f_i$ as described in the theorem below.

Theorem 1: If $\delta_1' = \delta_2'$, $\angle f_i$ is a quasi-concave function of i and its value ranges from $\frac{2\pi}{\lambda_c}(d_2 - d_1)$ to 0. If $d_1 = d_2$, $\angle f_i$ monotonically increases with respect to i, and is bounded in $[-2\pi\Delta_r(\delta_1' - \delta_2')N_r, 2\pi\Delta_r(\delta_1' - \delta_2')N_r]$.

When $\delta_1' = \delta_2'$, it means that two MSs are located in the same vertical direction perpendicular to the BS array, i.e., $\Delta_\omega = 0^\circ$, and $d_1 = d_2$ indicates that two MSs are in the same horizontal direction parallel to the BS array, $\Delta_\omega = 90^\circ$, see Fig. 2. In the former case $|d_1 - d_2|$ represents the physical spacing of the MSs in the vertical direction, and in the latter case $|(\delta_1' - \delta_2')N_r|$ is proportional to the MS spacing in the horizontal direction. Fixing the MSs spacing in the two cases, i.e., $|\Delta_r \lambda_c (\delta_1' - \delta_2')N_r| = |d_1 - d_2|$, from Theorem 1, we can see that the range of $\angle f_i$ is larger in the latter case than in the former case, as $2\pi\Delta_r |(\delta_1' - \delta_2')| N_r = \frac{2\pi}{\lambda_c} |d_1 - d_2|$. Thus it is more efficient to decorrelate MS channels by increasing the number of antennas in the latter case, i.e., when the MSs are in the same horizontal direction parallel to the BS

array. Furthermore, the saturation on phase variation still exists in these two cases. We illuminate this phenomenon with simulations in Sec. IV.

C. Pathloss Difference and Spatial Decorrelation

Due to analytical tractability, we have $f \leq \sum_{i=-\delta N_r}^{(1-\delta)N_r} |f_i| \leq 1$, and the equality holds if and only if $L_{1,i} = L_{2,i+(\delta_1'-\delta_2')N_r}$. Note that $|f_i| \propto 1/|L_{1,i}L_{2,i+(\delta_1'-\delta_2')N_r}|$ represents product of pathloss from each MS to the ith antenna, and $\sum_{i=-\delta N_r}^{(1-\delta)N_r} |f_i|$ is the normalized inner product of the vectors $\left[\begin{array}{ccc} \frac{1}{|L_{1,-\delta_1' N_r}|} & \cdots & \frac{1}{|L_{1,(1-\delta_1')N_r}|} \end{array}\right]$ and $\left[\begin{array}{ccc} \frac{1}{|L_{2,-\delta_2' N_r}|} & \cdots & \frac{1}{|L_{2,(1-\delta_2')N_r}|} \end{array}\right]$, which measures the difference between two MSs' pathloss over the array. In this section, our aim is to bound the channel correlation coefficient by this inner product and we have the results in the following.

Theorem 2 (Upper bound of correlation function): When $\delta_1' \neq \delta_2'$ and $\delta_1' > \delta_2'$, we have

1) $f(N_r, \Delta_r, \boldsymbol{\delta}; \theta, d, \Delta_u, \Delta_\omega) < A+B$, if $(\delta_1'-\delta_2') > 1/N_r$,
2) $f(N_r, \Delta_r, \boldsymbol{\delta}; \theta, d, \Delta_u, \Delta_\omega) < A+B'$, if $(\delta_1'-\delta_2') = 1/N_r$,
3) $f(N_r, \Delta_r, \boldsymbol{\delta}; \theta, d, \Delta_u, \Delta_\omega) < B'$, if $(\delta_1'-\delta_2') < 1/N_r$,

where

$$\begin{aligned} A &= C_0\left(\frac{d_2}{\sqrt{d_2^2+G^2}} + \frac{d_1}{\sqrt{d_1^2+G^2}}\right), \\ B &= \frac{d_1 d_2}{\Delta_r \lambda_c G}\left(\ln\left(\frac{G}{\Delta_r\lambda_c}+1\right)^{C_1}\left(\frac{G}{\Delta_r\lambda_c}-1\right)^{C_2}\right) + C_3, \\ B' &= C_1 \frac{d_1 d_2}{(\Delta_r\lambda_c)^2} + C_3, \\ G &= \Delta_r \lambda_c (\delta_1' - \delta_2') N_r, \end{aligned} \tag{26}$$

and C_0, C_1, C_2 and C_3 are constants.

The term $1/N_r$ is related to the angular resolution of a linear array which describes the ability of the array to resolve two rays. With spherical wave, if two MSs' horizontal spacing is smaller than $\Delta_r\lambda_c$, their channel correlation is determined by their vertical spacing. For $d_1 d_2$ in B and B', by mean value inequality, when $d_1 = d_2$, $d_1 d_2$ will be maximized subject to a fixed value of $\frac{d_1+d_2}{2}$. Thus decreasing the average BS-MS distance $\frac{d_1+d_2}{2}$ and at the same time increasing the vertical spacing of the MSs are beneficial to spatial decorrelation of the MS channels. We also observe that increasing the BS antenna spacing $\Delta_r\lambda_c$ rather than the antenna number can decrease the channel correlation.

IV. Simulation Results and Discussion

In this section, we investigate the channel correlation of two single-antenna MSs in LoS, using the proposed spherical-wave model. We study two typical scenarios – the included angle of two MSs 1) $\Delta_\omega = 90°$, where the MSs are on the line parallel to the BS antenna array, and 2) $\Delta_\omega = 0°$, where the MSs are on the line perpendicular to the BS antenna array, see Fig. 2.

In Fig. 3, we show the channel correlation of the MSs when the BS antenna spacing $\Delta_r = 1/2$ wavelengths and the MSs are at the edge (Fig. 3(a) and (b)), and at the middle (Fig. 3(c) and (d)) of a urban-macro cell. According to 3GPP TR36.873 [18], we choose the urban-macro cell radius to be 250 m, so the BS-MS distance is 250 m at the edge and 125 m at the middle of the cell. We see that the channel correlation between the MSs reduces as we increase the MS spacing or the number of BS antennas. As expected, the spatial separation is more difficult in the second scenario than in the first scenario, even with a very large number of antennas (up to a thousand), the correlation is quite high. Besides, when the MSs are at the middle of the cell, it is easier to separate them than when whey are at the edge.

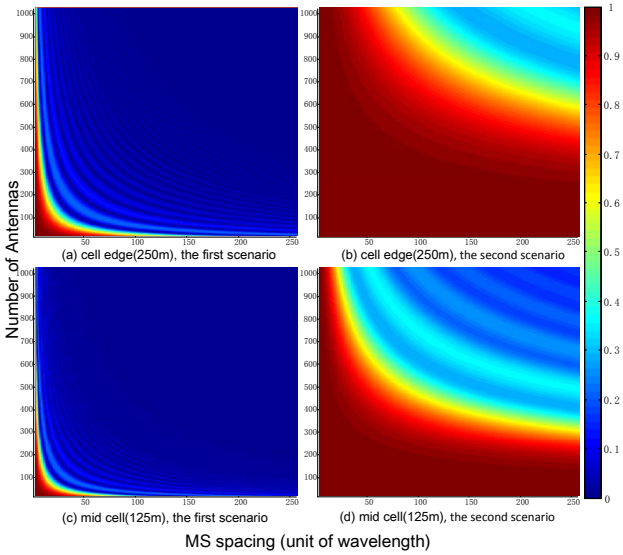

Fig. 3. Channel correlation between two MSs in LoS conditions in the two studied scenarios, when they are 250 m (at the edge of a cell) and 125 m (at the middle of a cell) away from the BS.

Fig. 4 illustrates that the channel correlation reduces with an increasing number of antennas, for different MS spacings. We can rely on increasing the number of antennas to separate the MSs before the saturation region is reached, as remarked in Theorem 1. We also observe ripples on the correlation coefficient as the antenna number increases. This is similar to the plane-wave model where the correlation coefficient is a sinc function of the antenna number [12].

In Fig. 5(a), we see that the MS channel correlation increases as the BS-MS distance increases, and it becomes more and more difficult to spatially separate the MSs, especially when their spacing is relatively small. In Fig. 5(b), we fix the aperture of the BS array to be $64\lambda_c$ and increase the number of antennas. We can see that in this case adding antennas does not help decorrelate the MSs.

Fig. 6 shows the MS channel correlation with LoS and one reflection path. The power ratio between the LoS path and the reflection path is set to $\kappa = 5$ dB. Comparing with Fig. 3, the reflection path helps reduce the channel correlation, especially in the second scenario that is particular difficult to separate the MSs. The effect of the reflection path is equivalent to having "virtual" BS antennas (see Fig. 1) which also contribute to the spatial separation.

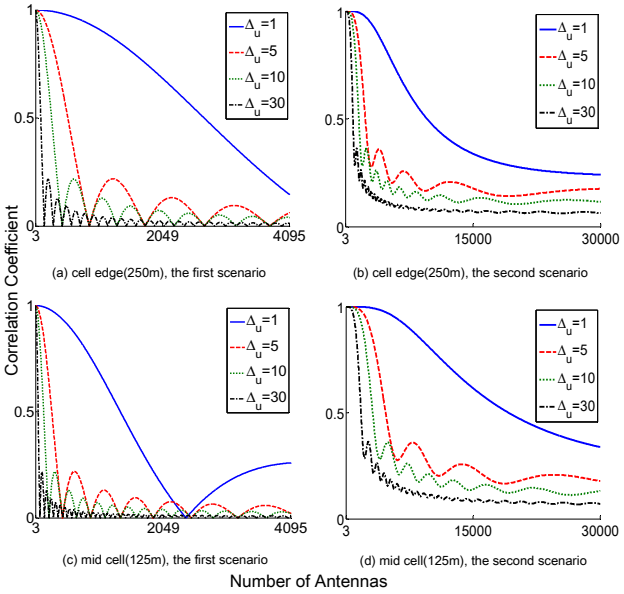

Fig. 4. Channel correlation as the number of antennas increases, for antenna spacing $\Delta_r = 1/2$ wavelengths and different MS spacings.

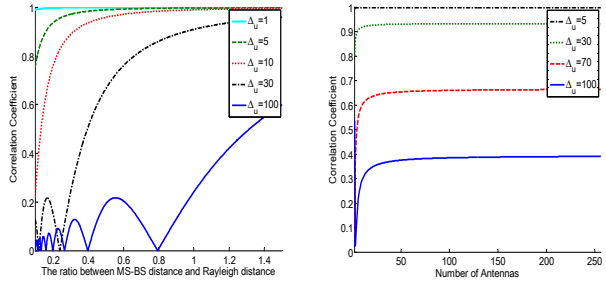

(a) $\Delta_r = 1/2$, $N_r = 128$, the first scenario

(b) Array aperture is $64\lambda_c$, $d = 125$ m, the first scenario

Fig. 5. (a) Channel correlation of the MSs with the BS-MS distance. (b) Channel correlation of the MSs with a fixed BS array aperture and varying number of antennas.

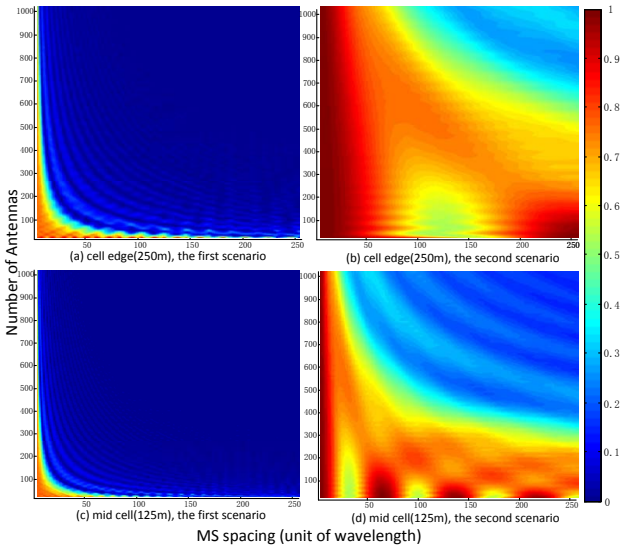

Fig. 6. Channel correlation in LoS condition with one reflection path, for the two studied scenarios, when the MSs are 125 m (at the middle of a cell) and 250 m (at the edge of a cell) away from the BS.

V. Conclusion and Future Work

Based on the proposed spherical-wave model, we investigated the channel correlation of two MSs in different settings. We illustrated how the spherical wavefronts can help decorrelate the MS channels. The spherical-wave model is compatible with the conventional plane-wave model, and can be extended to other types of array and the case of more MSs.

Acknowledgement

The authors would like to acknowledge the financial support from the Fund of High Level Academic Conference Program in the Graduate School of UESTC under Grant A1598521023901001.

References

[1] F. Rusek, D. Persson, B. K. Lau, E. Larsson, T. Marzetta, O. Edfors, and F. Tufvesson, "Scaling up MIMO: Opportunities and challenges with very large arrays," *IEEE Signal Process. Mag.*, vol. 30, no. 1, pp. 40–60, Jan. 2013.

[2] E. Larsson, O. Edfors, F. Tufvesson, and T. Marzetta, "Massive MIMO for next generation wireless systems," *IEEE Commun. Mag.*, vol. 52, no. 2, pp. 186–195, Feb. 2014.

[3] D. Gesbert, H. Bolcskei, D. GORE, and A. Paulraj, "Outdoor MIMO wireless channels: models and performance prediction," *IEEE Trans. Commun.*, vol. 50, no. 12, pp. 1926–1934, Dec. 2002.

[4] S. Payami and F. Tufvesson, "Channel measurements and analysis for very large array systems at 2.6 ghz," in *Antennas and Propagation (EUCAP), 2012 6th European Conference on*, Mar. 2012, pp. 433–437.

[5] X. Gao, F. Tufvesson, O. Edfors, and F. Rusek, "Channel behavior for very-large MIMO systems - initial characterization," in *COST IC1004, Bristol, UK*, Sept. 2012.

[6] ——, "Measured propagation characteristics for very-large MIMO at 2.6 ghz," in *2012 Conference Record of the Forty Sixth Asilomar Conference on Signals, Systems and Computers (ASILOMAR)*, Nov. 2012, pp. 295–299.

[7] X. Gao, O. Edfors, F. Rusek, and F. Tufvesson, "Massive MIMO performance evaluation based on measured propagation data," *IEEE Trans. Wireless Commun.*, vol. 14, no. 7, pp. 3899–3911, July 2015.

[8] X. Gao, O. Edfors, F. Tufvesson, and E. Larsson, "Massive MIMO in real propagation environments: Do all antennas contribute equally?" *IEEE Trans. Commun.*, vol. PP, no. 99, pp. 1–1, 2015.

[9] J. D. Kraus and R. J. Marhefka, "Antenna for all applications," Upper Saddle River, NJ: McGraw Hill, 2002.

[10] A. F. Molisch, *Wireless Communications*. John Wiley & Sons, 2007.

[11] *Requirements for Further Advancements for Evolved Universal Terrestrial Radio Access (EUTRA) (LTE-Advanced)*, Mar. 2009.

[12] D. Tse and P. Viswanath, *Fundamentals of Wireless Communication*. Cambridge University Press, 2005, ch. 7, pp. 229–326.

[13] P. Driessen and G. Foschini, "On the capacity formula for multiple input-multiple output wireless channels: a geometric interpretation," *IEEE Trans. Commun.*, vol. 47, no. 2, pp. 173–176, Feb. 1999.

[14] "Spherical wave model for short-range MIMO," *IEEE Trans. Commun.*, vol. 53, no. 5, pp. 905–905, May 2005.

[15] F. Bohagen, P. Orten, and G. Oien, "Design of optimal high-rank line-of-sight MIMO channels," *IEEE Trans. Wireless Commun.*, vol. 6, no. 4, pp. 1420–1425, Apr. 2007.

[16] ——, "On spherical vs. plane wave modeling of line-of-sight MIMO channels," *IEEE Trans. Commun.*, vol. 57, no. 3, pp. 841–849, Mar. 2009.

[17] H. Q. Ngo, E. Larsson, and T. Marzetta, "Aspects of favorable propagation in massive mimo," in *2014 Proceedings of the 22nd European Signal Processing Conference (EUSIPCO)*, Sept. 2014, pp. 76–80.

[18] *Study on 3D channel model for LTE*, 3GPP Std. TR 36.873, Rev. V12.0.0, 2014.